

**Figure 6** Measured phase of the field at the output of the five-tray structure at 10.5 and 12.5 GHz. (a) E-plane cut. (b) H-plane cut

as the distributing/combining device [5]. However, this has not been attempted here.

### 3. CONCLUSIONS

Theoretical and experimental investigations have been performed on the application of a uniplanar quasi-Yagi antenna as a receiving and transmitting antenna element of a spatial power combiner. A single tray consisting of two back-to-back antennas, and then five- and seven- tray configurations for operation in the *Ku*-band, have been developed. Using horn antennas to distribute and collect microwave power, the experiments have been performed in terms of return loss, insertion loss, and field uniformity across the trays to achieve optimal power-combining conditions. The results have shown that the investigated structures featured small insertion losses. Also, using ordinary horns, relatively high uniform excitation over a stack of trays has been achieved over a large frequency band. These overall results of the investigations indicate that the quasi-Yagi antenna is a suitable element to develop a broadband spatial power combiner.

### REFERENCES

1. J.A. Navarro and K. Chang, *Integrated active antennas and spatial power combining*, Wiley InterScience, New York, 1996.
2. R.A. York and Z.B. Popovic, *Active and quasi-optical arrays for solid-state power combining*, Wiley InterScience, New York, 1997.
3. N.-S. Cheng, P. Jia, D.B. Rensch, and R.A. York, A 120-W X-band spatially combined solid-state amplifier, *IEEE Trans Microwave Theory Tech* 47 (1999), 2557–2561.
4. Y. Qian, W.R. Deal, N. Kaneda and T. Itoh, A uniplanar quasi-Yagi antenna with wide bandwidth and low mutual coupling characteristics, 1999 IEEE AP-S Int Symp, July 1999, vol. 2, pp. 924–927.

5. T. Ivanov and A. Mortazawi, A two-stage spatial amplifier with hard horn feeds, *IEEE Microwave Guided Wave Lett* 6 (1996), 88–90.

© 2000 John Wiley & Sons, Inc.

## CHARACTERIZATION OF A WIDEBAND, LOW-Q, ELECTRICALLY SMALL ANTENNA

Craig A. Grimes,<sup>1</sup> Gang Liu,<sup>1</sup> Dale M. Grimes,<sup>1</sup> and Keat Ghee Ong<sup>1</sup>

<sup>1</sup> Department of Electrical Engineering  
University of Kentucky  
Lexington, Kentucky 40506-0046

<sup>2</sup> Department of Physics and Astronomy  
University of Kentucky  
Lexington, Kentucky 40506-0055

Received 30 March 2000

**ABSTRACT:** Using numerical and experimental techniques, a wideband, low-Q, electrically small antenna design is characterized as a function of frequency and the relative phasing between antenna elements. The antenna demonstrates wideband operation, with a radiation *Q* approximately a factor of 20 below the *Q*-limit established by Chu for electrically small, omnidirectional antennas. © 2000 John Wiley & Sons, Inc. *Microwave Opt Technol Lett* 27: 53–58, 2000.

**Key words:** radiation *Q*; electrically small antennas

### INTRODUCTION

Analytic work has shown that the radiation *Q* of certain multielement antennas is a function of the relative phasing between the different radiating elements [3]. The analytic work has recently been confirmed [2] both numerically and experimentally for the simplest of these designs, a turnstile antenna, comprised of two perpendicularly oriented collocated electric dipoles. The most intriguing antenna design discussed in [3] consists of four spatially collocated dipoles; two perpendicularly oriented magnetic (TE) dipoles are collocated with two perpendicularly oriented electric (TM) dipoles. The TE and TM dipole pairs are phased to support similarly directed circular polarization, and the pairs are driven  $\pi/2$  out of phase. For this source, the analytically predicted radiation *Q* is 0 [3] independently of the size-to-wavelength ratio. In this paper, we report on our attempts to confirm or deny the analytical predictions using numerical and experimental techniques.

Earlier attempts to build and characterize this antenna using a feed for each of the four dipoles were unsuccessful due to unwanted power transfer between adjacent, symmetrically located dipole feeds [5]. To avoid such difficulties, the four-dipole antenna was built using two separate dipole-pair elements, with each element supporting an equal power electric and magnetic moment; see Figure 1. Using this design, unwanted coupling between the feeds and the relative phasing between the two dipole-pair elements can be controlled. The radiation *Q* of the antenna system is determined using the numerical and experimental techniques detailed earlier [1, 2]. *Q*-values are obtained as a function of the phasing between the dipole pairs and the relative electrical size *ka*; a

Contract grant sponsor; U.S. Air Force Office of Scientific Research  
Contract grant number: Contract F49620-96-1-0353

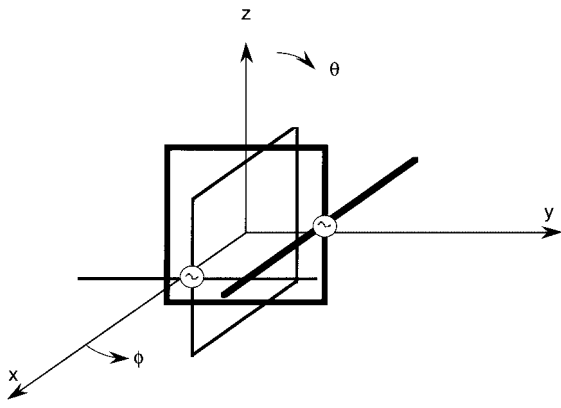


**Figure 1** Schematic drawing of antenna comprised of two dipole-pair elements, with each element providing equal-power TE and TM fields. Different line thicknesses are used to denote the two different dipole-pair elements

is the radius of the smallest virtual sphere that circumscribes the antenna, and  $k$  is the wavenumber of radiation equal to  $2\pi/\lambda$ .

### THEORETICAL MODEL

We define radiation  $Q$  by the equation [3]

$$Q = \frac{\omega W_{Spk}}{P} \quad (1)$$

$W_{Spk}$  denotes the peak standing-field energy that remains attached to the source, and  $P$  is the time average (real) output power. The historical difficulty with the calculation of antenna  $Q$  is determining which part of the total field energy remains associated with the source, returning to the antenna to determine radiation  $Q$ , and which part does not.

The analytic method for determining antenna  $Q$ , described in detail in [3] and summarized here, begins with the time-dependent Poynting vector  $\mathbf{N}$ , where boldface indicates a vector. The power that separates from the outgoing wave is calculated using the divergence of the power at constant retarded time  $t_R = t - \sigma/\omega$ , where  $t$  denotes time,  $\omega$  is the

radian frequency,  $\sigma = kr$ , and  $r$  is the radial distance from the source. The divergence at constant retarded time is equal to the rate at which energy is extracted from the wave at each point in four-space. An indefinite time integral of the result and the addition of the appropriate integration constant result in the source-associated standing-energy density  $W_{dS}(t_R)$ , where subscript  $d$  indicates density and  $S$  indicates source associated. The integration constant is chosen in such a way that it is both part of the total energy density  $W_{dT}(t_R) = (\epsilon/2)\mathbf{E} \cdot \mathbf{E} + (\mu/2)\mathbf{H} \cdot \mathbf{H}$  and the smallest possible value for which  $W_{dS}(t_R) \geq 0$  at all points in four-space. To find the peak source-associated standing energy [3]  $W_{Spk}$ : 1) determine the time-dependent Poynting vector  $\mathbf{N}$  for the radiation source, 2) evaluate the divergence of  $\mathbf{N}$  at constant retarded time, 3) take the indefinite integral of this divergence with respect to retarded time to obtain the time-varying portion of the source-associated standing energy density, 4) insert the smallest integration constant for which the source-associated standing energy is positive at all points in four-space, and 5) take the definite integral of the time-dependent source-associated standing energy density over external space to obtain  $W_S(t_R)$ , from which we obtain the peak value  $W_{Spk}$ .

It should be noted that all analytic techniques used to determine the radiation  $Q$  of a source [3, 4, 6] necessarily solve for the fields external to a virtual sphere enclosing the radiation source, and so ignore standing energy at radii less than the length of the antenna arms. Hence, the analytic expressions for  $Q$  are inherently optimistic in that the actual  $Q$  is undoubtedly higher due to standing energy within the antenna arm radius.

The analytic technique is applied to a spherical source consisting of four coherently radiating dipoles. Two special cases are examined.

Case A: An electric and magnetic dipole (dipole-pair) oriented along both the  $x$ - and  $y$ -axes. All four dipoles are driven in phase.

Case B: The  $x$ -axis directed dipole-pair are driven in time quadrature with the  $y$ -axis dipole-pair.

The radiation quantities of interest for Case A follow, beginning with the total instantaneous energy density:

$$W_{dT}(t_R) = \frac{\epsilon}{2} \left\{ 4 \left\langle \frac{1}{\sigma^6} [1 - \cos(2\omega t_R)] + \frac{2}{\sigma^5} \sin(2\omega t_R) + \frac{1}{\sigma^4} [1 + \cos(2\omega t_R)] \right\rangle \sin^2 \theta \right. \\ \left. + \left\langle \left( \frac{2}{\sigma^2} + \frac{1}{\sigma^6} \right) [1 - \cos(2\omega t_R)] - \left( \frac{4}{\sigma^3} - \frac{2}{\sigma^5} \right) \sin(2\omega t_R) + \frac{4}{\sigma^4} \cos(2\omega t_R) \right\rangle (1 + \cos^2 \theta) \right\} \quad (2)$$

where  $\epsilon$  is the permittivity of space. The spherical Poynting vector components are

$$\eta N_r(t_R) = \left\{ \frac{1}{\sigma^2} [1 - \cos(2\omega t_R)] - \left( \frac{2}{\sigma^3} - \frac{1}{\sigma^5} \right) \sin(2\omega t_R) \right. \\ \left. + \frac{2}{\sigma^4} \cos(2\omega t_R) \right\} (1 + \cos^2 \theta) \quad (3)$$

$$\eta N_\theta(t_R) = \left\{ \frac{4}{\sigma^4} \cos(2\omega t_R) \right. \\ \left. - \left( \frac{2}{\sigma^3} - \frac{2}{\sigma^5} \right) \sin(2\omega t_R) \right\} \sin \theta \cos \theta \quad (4)$$

$$N_\phi(t_R) = 0 \quad (5)$$

The source-associated standing energy density is

$$W_{ds}(t_R) = \frac{\varepsilon}{2} \left\{ 4 \left\langle \frac{1}{\sigma^6} [1 - \cos(2\omega t_R)] + \frac{2}{\sigma^5} \sin(2\omega t_R) + \frac{1}{\sigma^4} [1 + \cos(2\omega t_R)] \right\rangle \sin^2 \theta \right. \\ \left. + \frac{1}{\sigma^6} [1 - \cos(2\omega t_R)] (1 + \cos^2 \theta) \right\}. \quad (6)$$

Integrating (6) over all space, the total source-associated standing energy is

$$W_S(t_R) = \frac{8\pi\varepsilon}{3k^3} \left\{ \frac{1}{(ka)^3} [1 - \cos(2\omega t_R)] \right. \\ \left. + \frac{2}{(ka)^2} \sin(2\omega t_R) + \frac{2}{(ka)} [1 + \cos(2\omega t_R)] \right\} \quad (7)$$

The outbound real power is

$$p(t_R) = \frac{8\pi}{3\eta k^2} \left\{ [1 - \cos(2\omega t_R)] \right. \\ \left. - \left( \frac{2}{ka} - \frac{1}{(ka)^3} \right) \sin(2\omega t_R) \right. \\ \left. + \frac{2}{(ka)^2} \cos(2\omega t_R) \right\} \quad (8)$$

Combining (1), (7), and (8) the radiation  $Q$  of the source gives

$$Q = \frac{\omega W_{Spk}}{P_{av}} = \frac{1}{2(ka)^3} (1 + \sqrt{1 + 4(ka)^4}) + \frac{1}{(ka)} \quad (9)$$

where  $a$  is the radius of the source. For an electrically small antenna, the radiation  $Q$  of Case A is the same as that of a single electric dipole [3, 5].

For Case B the radiation properties are

$$W_{dT}(t_R) = \frac{\varepsilon}{2} \left\{ \frac{2}{\sigma^2} (1 + \cos^2 \theta) + \frac{4}{\sigma^4} \sin^2 \theta \right. \\ \left. + \frac{1}{\sigma^6} (2 + 3 \sin^2 \theta) \right\} \quad (10)$$

$$N_r(t_R) = \frac{1}{\eta} \left[ \frac{1}{\sigma^2} (1 + \cos^2 \theta) - \left( \frac{1}{\sigma^2} + \frac{1}{\sigma^6} \right) \cos \theta \right] \quad (11)$$

$$N_\theta(t_R) = -\frac{2}{\eta\sigma^5} \sin \theta \quad (12)$$

$$N_\phi(t_R) = \frac{2}{\eta} \left[ \left( \frac{1}{\sigma^3} + \frac{1}{\sigma^5} \right) - \frac{1}{\sigma^3} \cos \theta \right] \sin \theta \quad (13)$$

$$W_S(t_R) = 0 \quad (14)$$

$$P(t_R) = \frac{16\pi}{3\eta k^2} \quad (15)$$

$$Q = 0. \quad (16)$$

The calculated source-associated standing energy, and the resulting  $Q$ , are 0.

Keeping in mind that the  $Q = 0$  result is obtained using ideal, spherical mathematical functions, the result motivates both a numerical and experimental investigation of the source to see if a low- $Q$ , electrically small antenna can be realized.

## ANTENNA DESIGN AND CHARACTERIZATION TECHNIQUES

**Equal TM and TE Power from a Single Element.** For each antenna design (Fig. 1), an MoM analysis of a single element, shown in Figure 2, was performed to ensure that each element was radiating equal TE and TM power. The fields on the surface of the smallest virtual sphere that circumscribes the radiating elements were computed using NEC4 MoM. Following the approach described in [7], the calculated fields are equated to the multipolar field expansion to determine the TM dipole field coefficient  $F$  and the TE dipole field coefficient  $G$ . The TE-to-TM dipole power ratio is equal to  $(G/F)^2$  [7]. Figure 3 is the calculated TE/TM power ratio plot for the structure shown in Figure 2, with loop sides  $a = l/2 = 12$  cm. As shown in Figure 3, for these dimensions, the element radiates equal TE and TM power at 166.67

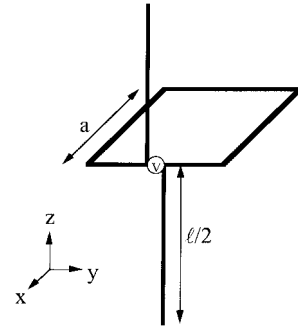


Figure 2 Single TE and TM dipole-pair element

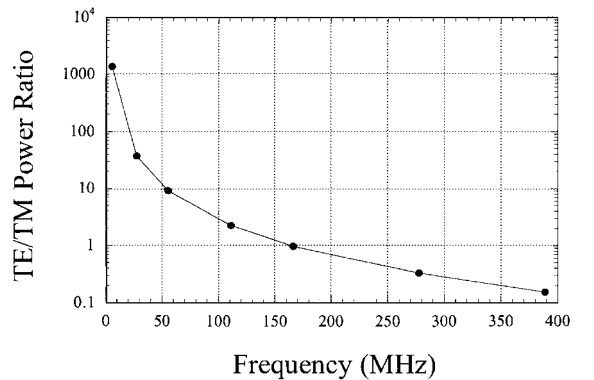


Figure 3 TE/TM power ratio versus frequency from single dipole-pair element pair shown in Figure 2, with dimensions  $a = l/2 = 12$  cm

MHz. Since the dimensions scale linearly with frequency for loop side  $a = l/2 = 4$  cm, the equal power frequency is 500 MHz.

**Numerical Determination of  $Q$ .** In earlier work [1, 2], a numerical technique was presented that is capable of accurately measuring the total source-associated standing energy, i.e., the energy that returns from the radiation field to the antenna and enters into the calculation of radiation  $Q$ . The numerical method for determining  $Q$  of an antenna is as follows. After attaining steady-state operation, the source driving voltage is turned off. After source turn off, the local standing-energy field collapses. The source-associated standing energy returns to the antenna, from which it is either reflected back into space or absorbed in the source resistor. After source turn off, the time integral of the power absorbed in the source resistor [1] and the time integral of the power reflected from the antenna back into space are summed. The sum is put equal to the source-associated standing energy.

The finite-difference time-domain (FDTD) technique for determining  $Q$  avoids spurious errors due to unwanted power reflections associated with feed networks, allowing for direct characterization of the antenna itself. This is of great importance for the antenna discussed herein, comprised of two radiating elements driven by a single generator through a power splitter and a feed network. When the voltage phase difference between the two elements is  $90^\circ$ , the operating point of interest, the waves reflected back from the two elements to the generator, are  $180^\circ$  out of phase, and cancel with the forward traveling wave. Zero reflected power is measured independently of antenna properties. Consequently, the time-domain method of determining radiation  $Q$  [2] is employed in this work so that antenna performance can be characterized independently of transmission-line effects.

The FDTD computations were made using a rectangular, three-dimensional computer code based on the Yee [8–10] cell. The problem space was chosen as  $120 \times 120 \times 120$  cells, with cell dimensions  $\Delta x = \Delta y = \Delta z = 5$  mm; a perfectly matched absorbing boundary layer was used to terminate the computational space [11]. As described previously [1, 2], the antenna elements are fed with a modified sinusoidal wave of frequency  $f$  [12, 13] to cancel spurious transient computations. Each element (see Fig. 2) is composed of a square loop and a straight-wire electric dipole. For the numerical computations, the dimensions of the antenna were held constant at loop side length 12 cm and electric dipole length 24 cm. The operational frequency was varied above and below 166.67 MHz, the frequency at which the TE and TM powers are of equal magnitude.

**Experimental Determination of  $Q$ .** An analogous technique is used to experimentally determine antenna  $Q$  [2]. The network for characterization of the antenna is shown in Figure 4, with a circulator placed in the feed line of each element. After steady-state operation is reached, the generator is turned off, and the power is returned to each element captured from the output of the circulators using a two-channel oscilloscope. The returned power from each element is integrated over time, and then summed. That quantity is set equal to the source-associated standing energy. The output real power  $P$  is determined using a network analysis of the feed system. In common with the numerical analysis, the experimental  $Q$  measurement technique isolates antenna

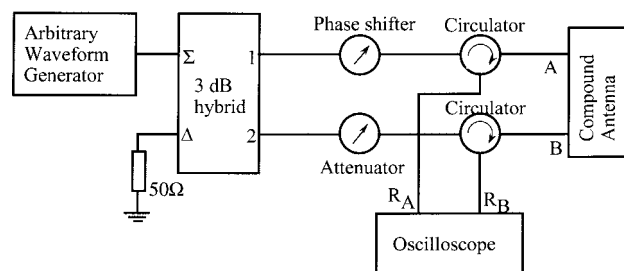


**Figure 4** Experimental setup for measuring radiation  $Q$  of antenna shown in Figure 1

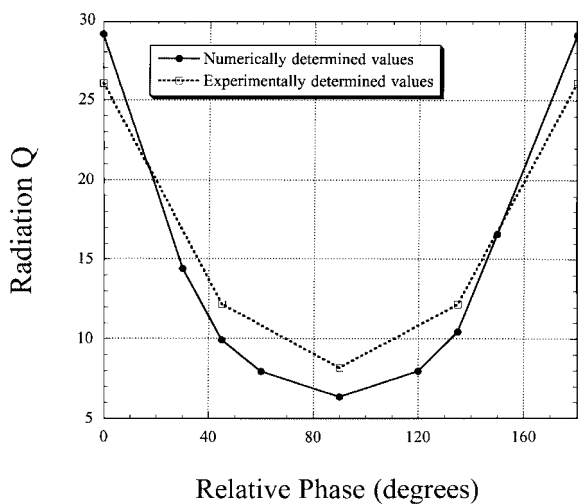
performance from the feed network, enabling direct characterization of the antenna.

A Tektronix arbitrary waveform generator (AWG610) is used as the source generator. The AWG610 is able to generate an arbitrary waveform to 500 MHz, and to terminate the waveform virtually without a measurable transient. The generator output power in steady state can be determined from the measured voltage, and is calculated to be about 7.1 mW (8.5 dBm). The circulator effectively divides the input and reflected signals, so the generator always sees the network as a  $50 \Omega$  load, and delivers the same power as calculated above. A 3 dB hybrid is used to split the power between two dipoles, a phase shifter to adjust the desired phase difference, an attenuator to compensate for the loss in the phase shifter, and circulators to separate the incoming and reflected signals. To capture the transient signal coming back from the antenna elements upon source shutdown, an 8 Gsample/s HP 54845A oscilloscope is used. The antenna is a two-port network, the scattering parameters of which are measured by a network analyzer. The scattering parameters of a five-port network (six with the hybrid port connected to  $50 \Omega$ ) are measured; all components in our experimental setup are  $50 \Omega$  devices. Using network theory, the power radiated by the antenna is determined taking into account any parasitic coupling between the two antenna elements. The total source-associated standing energy of the antenna is determined by summing the time integrals of reflected powers from each antenna element. A thin-wire antenna of loop side  $a = l/2 = 4$  cm was built and tested in an anechoic chamber.

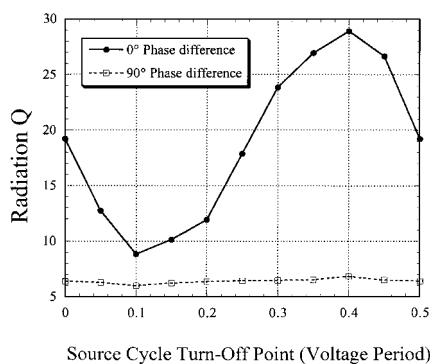
## RESULTS

Figure 5 shows the numerically and experimentally determined radiation  $Q$  of the antenna at  $ka = 0.42$  as a function of the phase difference between elements. In agreement with theory, the results show that the radiation  $Q$  is dependent upon relative phasing between the two antenna elements. In agreement with theory, when the dipoles are in phase, the  $Q$  is approximately that of an electric dipole [1, 3] of the same electrical size. When the dipole-pair elements support circular polarization, antenna  $Q$  is reduced by an approximate factor of 4.5 from the in-phase results. For this relative electrical size, the measured  $Q$ -value is approximately a factor of 3 below the minimum  $Q$ -value determined by Chu [4] for an omnidirectional antenna with the same  $ka$ -value.

Figure 6 shows the FDTD-determined radiation  $Q$  of the antenna for which  $ka = 0.42$  as a function of source turn-off point, relative to the minimum input power point [2]. Theory indicates that the source-associated standing energy is time varying for all relative phases except  $90^\circ$ , when the dipole



**Figure 5** Numerically and experimentally determined  $Q$  versus relative phase between dipole-pair elements;  $ka = 0.42$

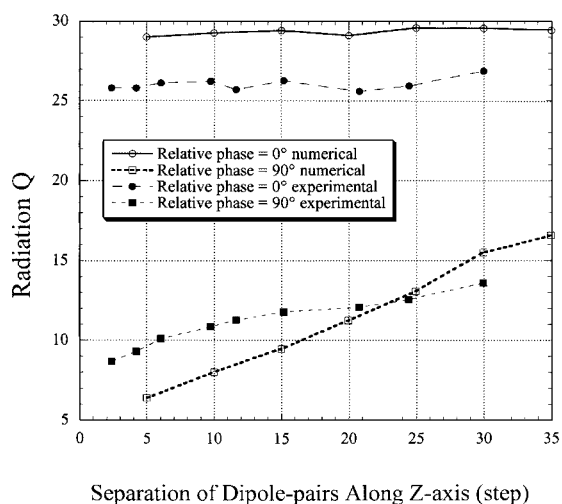


**Figure 6** Numerically determined  $Q$  as a function of source turn-off point, referenced to the input power minimum, for dipole-pair elements in phase and phased to support circular polarization;  $ka = 0.42$

pairs support circular polarization. As seen in Figure 6,  $Q$  is independent of the source turn-off point when circular polarization is maintained. However, for other relative phases,  $Q$  varies with the source turn-off point. As indicated by Eq. (1), the correct value of  $Q$  is the largest value that is determined when the source-associated standing energy is a maximum.

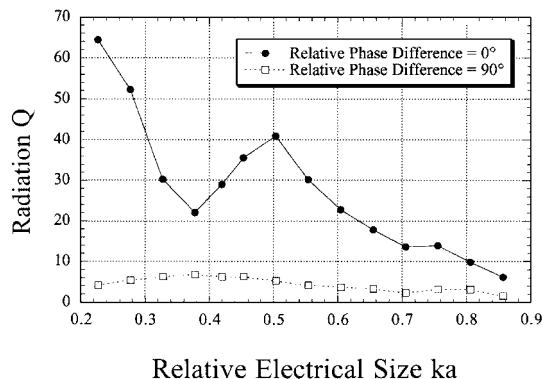
Figure 7 shows measured and computed  $Q$  versus relative space shift steps ( $D_z$ ) for antennas with  $ka = 0.42$ . Steps of 5 mm were taken in the numerical model, dimensions  $a = l/2 = 12$  cm, and steps of 1.67 mm were taken in the experimental work, dimensions  $a = l/2 = 4$  cm. Figure 7 illustrates what happens when, rather than being collocated, the source pairs are separated by distance  $D_z$  along the  $z$ -axis. With  $90^\circ$  relative phasing between the dipole-pair elements, the radiation  $Q$  is small for  $D_z$  small, and increases with increasing values of  $D_z$ . In contrast, when the four dipoles are in phase, the radiation  $Q$  is approximately that of an electric dipole of the same  $ka$  independently of  $D_z$  [3]. Further experiments moving the dipole pairs relative to each other in three dimensions showed similar results; the  $Q$  of the  $90^\circ$  phased dipole pair is sensitive to the relative location, and the  $Q$  of the in-phase dipole pairs is not.

Figure 8 shows the numerically determined  $Q$  versus relative phasing between dipole-pair elements and the rela-



**Figure 7** Numerically and experimentally determined  $Q$  as a function of spacing between dipole-pair elements,  $ka = 0.42$ . Step size = 5 mm in numerical model, 1.67 mm in experimental work

tive electrical size of the antenna. The trends seen in the numerical results have been confirmed experimentally over a more limited range,  $ka = 0.37$  to  $ka = 0.42$ , due to the inherent narrowband performance of the circulator. At  $ka = 0.23$ ,  $Q$  for the circularly polarized antenna is more than a factor of 20 below the Chu limit [4] for omnidirectional antennas. The oscillations seen in the in-phase  $Q$  results were reported earlier [1, 2, 15], and are due to higher order modes that cause variations in the outbound real power. The in-phase results clearly show the  $1/(ka)^3$  dependence of  $Q$  as the antenna becomes electrically small. In contrast, with the two dipole-pair elements phased to support circular polarization,  $Q$  is relatively insensitive to frequency. As noted earlier, when circular polarization is maintained, the antenna does not have to support, i.e., store in the near fields, large amounts of source-associated standing energy [3]. As discussed in [16, 17], the frequency response seen in Figure 8 is indicative of the fact that the current and charge distributions on the dipole-pair elements self-adjust to support radiation fields that minimize source-associated standing energy, and hence  $Q$ .



**Figure 8** Numerically determined  $Q$  of antenna, dimensions  $a = l/2 = 12$  cm, as a function of relative phasing between dipole-pair elements and electrical size  $ka$

## CONCLUSIONS

Earlier theoretical work [3, 14] showed the potential for a low- $Q$  electrically small antenna. In [3], analytic results showed a radiation source with  $Q = 0$  independently of the size-to-wavelength ratio. The antenna is comprised of four spatially collocated dipoles radiating equal powers: two perpendicularly oriented magnetic (TE) dipoles collocated and coaxial with two perpendicularly oriented electric (TM) dipoles. The TE and TM dipole pairs are phased to support circular polarization, and the TE and TM dipole pairs in phase with each other. In this work, the mathematics [3] were translated to thin wire antennas, and the radiation  $Q$  was determined both experimentally and numerically as a function of phasing between the two dipole-pair elements and frequency.

In agreement with theory [3], both experimental and numerical analyses show that the radiation  $Q$  of the antenna is a function of the relative phasing between dipole pairs, with the minimum value obtained when the dipole pairs are phased to support circular polarization. The measured and numerically determined  $Q$ -values are well below (by an approximate factor of 20 at  $ka = 0.23$ ) the limit established by Chu [4] for electrically small omnidirectional antennas. Furthermore, when phased to support circular polarization, the antenna demonstrates wideband operation.

## REFERENCES

1. G. Liu, C.A. Grimes, and D.M. Grimes, A time domain technique for determining antenna  $Q$ , *Microwave Opt Technol Lett* 21 (1999), 393–395.
2. C.A. Grimes, G. Liu, F. Tefiku, and D.M. Grimes, Time domain measurement of antenna  $Q$ , *Microwave Opt Technol Lett* 25 (2000), 95–100.
3. D.M. Grimes and C.A. Grimes, Radiation  $Q$  of dipole generated fields, *Radio Sci* 34 (1999), 281–296.
4. L.J. Chu, Physical limitations of omni-directional antennas, *J Appl Phys* 19 (1948), 1163–1175.
5. F. Tefiku and C.A. Grimes, Coupling between elements of electrically small compound antennas, *Microwave Opt Technol Lett* 22 (1999), 16–21.
6. J. McLean, A re-examination of the fundamental limits on the radiation  $Q$  of electrically small antennas, *IEEE Trans Antennas Propagat* 44 (1996), 672–676.
7. K.G. Ong and C.A. Grimes, A method for quantifying the higher order modes radiated by an arbitrarily shaped antenna, *Microwave Opt Technol Lett* 24 (2000), 20–24.
8. K.S. Yee, Numerical solution of initial boundary value problems involving Maxwell's equations in isotropic media, *IEEE Trans Antennas Propagat* AP-14 (1966), 302–307.
9. K.S. Kunz and R.J. Luebbers, *The finite difference time domain method for electromagnetics*, CRC Press, Boca Raton, FL, 1993.
10. A. Taflove, *Advances in computational electrodynamics: The finite-difference time-domain method*, Artech House, Norwood, MA, 1998.
11. J.P. Berenger, A perfectly matched layer for the absorption of electromagnetic waves, *J Comput Phys* 114 (1994), 185–200.
12. U. Kangro and R. Nicolaidis, Spurious fields in time-domain computations of scattering problems, *IEEE Trans Antennas Propagat* 45 (1997), 228–234.
13. G. Liu, K.G. Ong, C.A. Grimes, and D.M. Grimes, Comparison of time and frequency domain numerical modeling of outbound and local power from two perpendicularly oriented, electrically small TM dipoles, *Int J Numer Modeling* 12 (1999), 229–241.
14. D.M. Grimes and C.A. Grimes, Power in modal radiation fields: Limitations of the complex Poynting theorem and the potential for electrically small antennas, *J Electromag Waves Appl* 11 (1997), 1721–1747.

15. V. Badii, K. Tomiyama, and D.M. Grimes, Biconical transmitting antennas, A numerical analysis, *J Appl Comput Electromag Soc* 5 (1990), 62–92.
16. D.M. Grimes and C.A. Grimes, Bandwidth and  $Q$  of antennas radiating TE and TM modes, *IEEE Trans Electromag Compat* 37 (1995), 217–226.
17. D.M. Grimes and C.A. Grimes, Classical electrodynamics on an atomic scale of dimensions: Why a quantum theory of radiation is unnecessary, *Speculations Sci Technol* 20 (1997), 197–210.

© 2000 John Wiley & Sons, Inc.

## NOVEL MEANDERED PLANAR INVERTED-F ANTENNA FOR TRIPLE-FREQUENCY OPERATION

Wei Ping Dou<sup>1</sup> and Y. W. M. Chia<sup>1</sup>

<sup>1</sup> Centre for Wireless Communications  
Singapore 117674

Received 7 April 2000

**ABSTRACT:** A novel meandered planar inverted-F antenna with a single feed is presented for triple-frequency operation. Using two shorting strips, good impedance matching is achieved in three bands. This compact low-profile design shows characteristics of near-omnidirectional radiation patterns with minimal hand effects, which is preferable for application in wireless communications. © 2000 John Wiley & Sons, Inc. *Microwave Opt Technol Lett* 27: 58–60, 2000.

**Key words:** planar inverted-F antenna; meandered antenna; triple-frequency operation; finite-difference time-domain method

## 1. INTRODUCTION

The planar inverted-F antenna (PIFA) has been proposed as a candidate for portable wireless terminals because of its compactness. Recently, several multifrequency antennas arising from the PIFA have been presented [1–3]. For triple-frequency operation, Song et al. have presented three designs [3]. The first design was realized with a simple inverted-F antenna using three feeds. The second design, a dual-feed PIFA, was achieved by embedding an L-shape spur line as a reactive load. The third design, a single-feed PIFA, used two L-shape spur lines. In this letter, we propose a novel meandered PIFA with a single feed to operate at three frequency bands. Electric field distribution, return loss, bandwidth, and radiation patterns of the new design are investigated numerically and experimentally. The finite-difference time-domain method has been used for numerical simulation. In addition, the presence of a hand on the antenna performance is discussed.

## 2. ANTENNA DESIGN AND RESULTS

The proposed antenna is mounted on a finite ground plane (Fig. 1). It is well matched to a 50  $\Omega$  coaxial line using two shorting strips,  $G_1$  and  $G_2$ . Two linear slots,  $S_1$  and  $S_2$ , are cut in the patch. For this triple-frequency structure, we have found that the dimensions of  $S_1$  determine the highest resonant frequency, and the next resonance is mainly dependent on the dimensions of  $S_2$ . The highest resonant frequency decreases with a narrower width or a longer length of  $S_1$ . The frequency ratio can be adjusted in the range 1.05 ~ 2.11. The patch size depends on the lowest resonant frequency [2].